



## Impact of steam generator start-up limitations on the performance of a parabolic trough solar power plant

Ferruzza, Davide; Topel, Monika; Laumert, Björn; Haglind, Fredrik

*Published in:*  
Solar Energy

*Link to article, DOI:*  
[10.1016/j.solener.2018.05.010](https://doi.org/10.1016/j.solener.2018.05.010)

*Publication date:*  
2018

*Document Version*  
Peer reviewed version

[Link back to DTU Orbit](#)

*Citation (APA):*  
Ferruzza, D., Topel, M., Laumert, B., & Haglind, F. (2018). Impact of steam generator start-up limitations on the performance of a parabolic trough solar power plant. *Solar Energy*, 169, 255-263.  
<https://doi.org/10.1016/j.solener.2018.05.010>

---

### General rights

Copyright and moral rights for the publications made accessible in the public portal are retained by the authors and/or other copyright owners and it is a condition of accessing publications that users recognise and abide by the legal requirements associated with these rights.

- Users may download and print one copy of any publication from the public portal for the purpose of private study or research.
- You may not further distribute the material or use it for any profit-making activity or commercial gain
- You may freely distribute the URL identifying the publication in the public portal

If you believe that this document breaches copyright please contact us providing details, and we will remove access to the work immediately and investigate your claim.

# 1 **Impact of steam generator start-up limitations on the performance of a** 2 **parabolic trough solar power plant**

3 Davide Ferruzza<sup>1</sup>, Monika Topel<sup>2</sup>, Björn Laumert<sup>2</sup>, Fredrik Haglind<sup>1</sup>.

4 <sup>1</sup>Department of Mechanical Engineering, Technical University of Denmark, Nils Koppels Allé, Building  
5 403, 2800 Kongens Lyngby, Denmark

6 <sup>2</sup>Department of Energy Technology, KTH Royal Institute of Technology, 100 44, Stockholm, Sweden

7 \*Phone number: +45 27296900, e-mail: *daferr@mek.dtu.dk*

## 8 **Abstract**

9 Concentrating solar power plants are an attractive option in the renewable energy generation market. The  
10 possibility of integrating relatively cheap forms of energy storage makes them a desirable solution when  
11 power generation must be readily available at any time of the day. Solar power plants typically start-up  
12 and shut down every day, so in order to maximize their profitability, it is necessary to increase their  
13 flexibility in transient operation and to initiate power generation as rapidly as possible. Two of the key  
14 components are the steam generator and steam turbine and the rates at which they can reach operational  
15 speed are limited by thermo-mechanical constraints. This paper presents an analysis of the effects of the  
16 thermal stress limitations of the steam generator and steam turbine on the power plant start-up, and  
17 quantifies their impact on the economy of the system. A dynamic model of a parabolic trough power plant  
18 was developed and integrated with a logic controller to identify start-up limitations, and subsequently the  
19 dynamic model was integrated in a techno-economic tool previously developed by the authors. The plant  
20 was analysed under two different operating strategies, namely solar-driven and peak-load. The results  
21 indicate that for steam generator hot start-ups, a 1.5 % increase in peak-load electricity production would  
22 be achieved by doubling the maximum allowable heating rate of the evaporator. No useful increase would  
23 be achieved by increasing the rates beyond a limit of 7-8 K/min, as the turbine would then be the main

24 limiting component during start-up. Similar conclusions can be drawn for the solar-driven case, for which  
25 the solar field and the energy source availability would pose the major constraint when starting up the  
26 steam generator system.

27 **Key words:** *Solar Energy, Concentrating Solar Power, Parabolic Trough power plant; Steam generator;*  
28 *Steam turbine; Start-up;*

## 29 **Nomenclature**

30 ACC Air cooled condenser

31 CSPP Concentrating Solar Power plant

32 CT Cold tank

33 D Deaerator

34 ECO Economizer

35 EVA Evaporator

36 HP High pressure

37 HT Hot tank

38 HTF Heat transfer fluid

39 HX Heat exchanger

40 IHX Indirect heat exchanger

41 LCF Low Cycle Fatigue

42 LP Low pressure

43 PB Power block

44	PI	Proportional-Integral	
45	PTPP	Parabolic trough power plant	
46	RH	Re-heater	
47	SF	Solar field	
48	SGS	Steam generator system	
49	SH	Super-heater	
50	SM	Solar multiple	
51	ST	Steam turbine	
52	TES	Thermal Energy Storage	
53	<b>Symbols</b>		
54	ITD	Inlet Temperature Difference	[°C]
55	$\dot{m}$	Mass flow	[kg/s]
56	p	Pressure	[bar]
57	T	Temperature	[°C]
58	t	Time	[s]
59	$v_T$	Allowable ramp-up rate/heating rate	[K/min]
60	<b>Subscripts</b>		
61	f	fluid	
62	max	maximum	
63	min	minimum	

64 **1. Introduction**

65 Concentrated solar power plants (CSPPs) are becoming more common in the renewable energy market.  
66 This trend is expected to rise in the upcoming years due to their key capability of being integrated with  
67 relatively cheap thermal energy storage (International Energy Agency, 2014). This feature makes it  
68 possible to decouple the energy generation from the solar input, making the power they can generate  
69 available at any time (Guedez et al., 2017). However, despite this characteristic feature, CSPPs are not  
70 currently designed for continuous operation, therefore they still experience daily start-ups and shut-  
71 downs. In order to maximize their performance from both technical and economical standpoints,  
72 increasing the flexibility of their dynamic performance is an important aspect which must be addressed  
73 (Topel et al., 2017). The rate at which a power plant can start up is limited by thermo-mechanical  
74 constraints, which may increase the time to reach the nominal load of the power plant. The receiver, the  
75 steam turbine and the steam generator system (SGS) are usually the most limiting components in this  
76 regard. While the receiver (Samanes and Garcia-Barberena, 2014) and steam turbine (Topel et al., 2017)  
77 have been examined in the literature, the steam generator has not been the focus of many studies .

78 Many CSPPs in use today have steam generators which were typically designed as conventional heat  
79 exchangers, not optimised for transient applications (Vant-Hull, 2012). As the industry mainly used  
80 designs from conventional power plants, their SGS responded inefficiently to sudden changes in incident  
81 solar radiation and equally poorly to repeated morning start-ups. This can cause failures in the component  
82 due to excessive thermal stresses, which may compromise the economic viability of the power plants.  
83 Although the industry is interested in optimising SGS designs for CSPPs (Pelagotti et al., 2014), there is  
84 little information on optimal heating rate requirements. In order to maximize the flexibility (i.e. to  
85 increase the responsiveness of the power plant to a change in the power load or in insolation), and both  
86 the peak and the baseline rate of electric power production, it is essential that all the components are able  
87 to start as quickly as possible and enable the CSPPs to quickly start harvesting the incoming solar  
88 radiation. On the other hand, there might be limiting factors for one component, which might reduce the  
89 required heating rate for another. For example, if the receiver or solar field are the limiting factors, there  
90 is no need for the SGS to be able to start up at a faster rate than that of the solar field (Ferruzza et al.,  
91 2017).

92 The SGS and steam turbine both start up at a rate that is governed by the need to limit thermal stresses  
93 and low-cycle fatigue (LCF) (Pelagotti et al., 2014; Topel et al., 2017). Thick-walled components,  
94 material properties and temperature gradients are the limiting factors. In the case of the steam generator,  
95 the main constraining factors are the maximum allowable stresses in thick walled components such as the  
96 steam drum, super-heater headers and T or Y junctions in the steam pipelines (Dzierwa and Taler, 2014;  
97 Taler et al., 2015). Typically, the limiting component is the evaporator drum, which is designed as a large  
98 diameter high pressure vessel, which must consequently have thick walls. The start-up procedure of the  
99 component is intended to reach nominal conditions for temperature, pressure and mass flow rates as  
100 rapidly as possible. In the case of the steam turbine, the shaft seal and blading clearances determine the  
101 maximum allowable thermal expansion of the components, while the shaft thickness is the limiting factor  
102 for thermal stress. As a general rule, the starting procedure of a steam turbine can be considered to have  
103 three different phases: pre start-up heating, rolling up and loading up. During this procedure, the key  
104 parameter which limits the heating rate is the difference in temperature between the incoming steam and  
105 the metal of the turbine. In order to avoid excessive thermal stresses in this component it is desirable to  
106 keep the temperature difference as low as possible (Spelling et al., 2012).

107 In previous studies, much attention is given to the thermal stress that limits the maximum heating rates of  
108 these components, but little information is available about their impact on the performance of the overall  
109 power plant. For instance, González-Gómez et al. (2017) analysed the thermo-mechanical stress in the  
110 case of SGS for solar applications, but the study was performed at component level, without considering  
111 the impact of such limitations on the performance of the power plant. The author also focused on design  
112 and cost-based optimization of such components without considering the system perspective.

113 The abovementioned studies considered the limitation regarding either the steam generator or the turbine,  
114 without addressing the interaction between the two (Dzierwa et al., 2016; Dzierwa and Taler, 2014; Taler  
115 et al., 2015). It is of crucial importance to evaluate how much different constraints on the start-up  
116 procedures of CSPPs affect their electric power production and whether significant differences occur  
117 under different conditions. This information will indicate where to improve the operation of the power  
118 plant and the design specifications for the components, from a thermo-mechanical point of view. Lastly,  
119 the operational strategy of the power plant determines the number of start-ups and their typology (hot,  
120 warm or cold start-ups) (Guedez et al., 2017; Spelling et al., 2012). For instance, if a CSPP operates

121 purely in solar-driven without fuel back-up, its start-up would mainly occur in the morning when the sun  
122 is still rising. On the other hand, if a power plant is designed to work in peak load during a particular time  
123 of the day (e.g. during evening hours, when the price of electricity is higher), the start-up would occur  
124 when solar radiation or heat from the storage are readily available. From a start-up perspective (in the  
125 absence of back-up fuels), this would mean different availability of heat input, hence different start-up  
126 constraints.

127 The dynamic performance of parabolic trough power plants has been analysed previously (Almasabi et  
128 al., 2015; Blanco et al., 2011; Conrado et al., 2017; Luo et al., 2015), although the models proposed deal  
129 only with validation of the detailed component modelling of the solar field. Blanco et al. (2011)  
130 presented a model of a parabolic trough power plant (PTPP) and validated it against experimental data,  
131 but in this case the model of the power block was developed with a simplified correlation. Another  
132 approach was presented by Abed et al. (2016), in which a detailed dynamic model in APROS (Advanced  
133 Process Simulation Software) was validated against the operational data of Andasol II. The focus of the  
134 study was to develop a detailed control strategy of the power plant by means of PI (Proportional-Integral)  
135 controllers. The model presented did not focus on yearly performance but on daily control. None of these  
136 studies considered start-up constraints due to thermo-mechanical limitations. In previous works such  
137 constraints were usually analysed from a component perspective. For instance, Pelagotti et al. (2014)  
138 described in detail a dynamic model of a steam generator, and carried out a low-cycle fatigue analysis.  
139 The authors predicted the impact on the annual electricity production of PTPPs. Their calculations did not  
140 take into account start-up schedules of steam turbines or rates of heat availability, nor yearly performance  
141 evaluation of such power plants. A previous work by the authors (Topel et al., 2015) considered the  
142 impact of the start-up rate of the steam turbine for solar tower direct steam generation; however, in this  
143 work the start-up constraints of the steam turbine were not coupled with SGS constraints.

144 This paper presents an analysis of the effects of the thermal stress limitations of the steam generator  
145 and steam turbine on the power plant start-up, and quantifies their impact on the economy of the system.  
146 The study was performed for both solar-driven and peak-load conditions to emphasize on how different  
147 constraints on starting up a steam generator have different impacts on the electric power production and  
148 depend on how the plant is operated (Guedez et al., 2017). The paper also considers how differently sized

149 solar fields (in terms of solar multiple) affect the impact of the steam turbine and steam generator  
150 constraints from an operational perspective.

151 In section 2 the paper presents the approach used for modelling the power plant. Secondly, it  
152 summarizes the main limitation for the start-up of the steam generator and turbine and how such  
153 constraints were implemented in the control logic for the overall model. In section 3, it presents the  
154 evaluation of the impact of the constraints of the steam generator on the electric power production both in  
155 peak-load and solar-driven together with a discussion on the results. Lastly section 4 outlines the  
156 conclusions and final remarks.

## 157 2. Methods

158 Modelling was performed in DYESOPT, an in-house tool developed at KTH, Royal Institute of  
159 Technology, Stockholm, which was developed for techno-economic modelling of CSP plants (Guedez et  
160 al., 2017). The tool has been validated against Thermoflex, a commercially available software for power  
161 plant performance estimation (Thermoflow, 2014), demonstrating a relative deviation between the results  
162 of two software below 10 % in the case considered. As may be seen in Figure 1, the tool allows for both  
163 steady-state design and dynamic simulation, and can make techno-economic calculations for different  
164 assumed locations for the plant. The overall approach, as shown in Figure 1, can be linked to a multi-  
165 objective optimizer (Guedez et al., 2017).

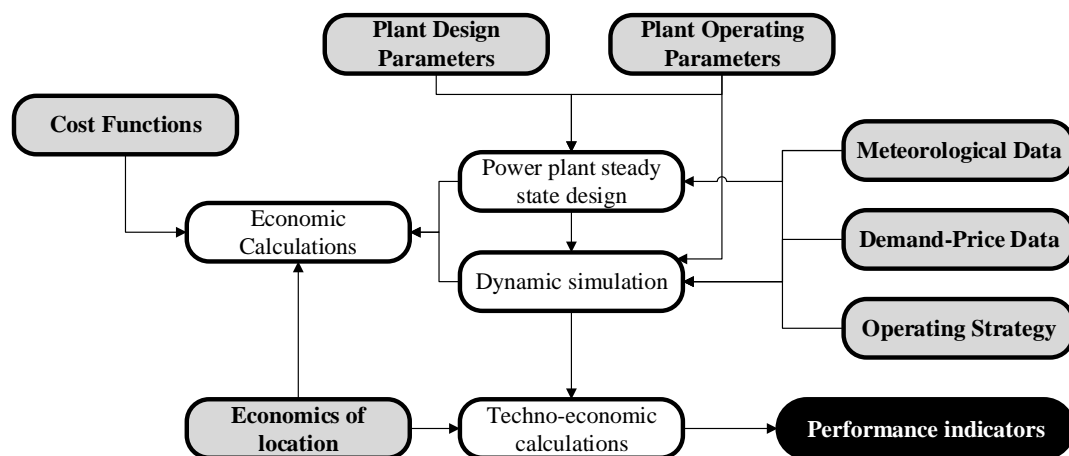


Figure 1: DYESOPT workflow diagram.

166 The model of the PTPP was implemented in the tool and validated as described in Ferruzza et al., (2015).  
167 The author implemented the parabolic trough sizing methodology and the TRNSYS model in DYESOPT  
168 and validated against data available in literature with a maximum error of -8.9 % (Ferruzza et al., 2017).



169 The model was further developed by including different operating strategies and the option of including  
 170 an air-cooled condenser (ACC). The consideration of ACCs is of topical interest, as many plants that are  
 171 currently under development or in the tender phase will be placed in desert areas. Having no direct access  
 172 to cooling water mandates the use of ACC in which the condensation of steam is achieved solely by air  
 173 cooling and parasitic electrical power consumption (Moore et al., 2013). The ACC model was previously  
 174 validated by Guedez et al. (2017).

## 175 **2.2 Steam generator start-up limitations**

176 The start-up procedure for a steam generator consists of bringing temperature, pressure and mass flow  
 177 rate to nominal values in each component of the system. As noted above, the rate at which this can be  
 178 done is highly dependent on thermo-mechanical limitations that are determined by their materials and  
 179 geometry. Previous studies have shown that the main limiting components during an SGS start-up are the  
 180 evaporator and super-heater, hence these two were considered in detail in the present study (Basaran,  
 181 2015; Taler et al., 2015). Another constraint which must be addressed is the occurrence of thermal shocks  
 182 that might occur if the HTF temperature is higher than the metal temperature by more than a critical  
 183 amount, as the material could then experience cracking and ultimately failure (Price, 2017). A limit on the  
 184 maximum allowable temperature difference is usually implemented in the control logic of the start-up  
 185 operation. Even though the minimum and maximum heating rates  $v_{T_{\min}}$  and  $v_{T_{\max}}$  for the required pressure  
 186 can be determined according to the norm DIN EN 12952-3 (CEN, 2012), the goal of the present study is  
 187 to determine the optimal range of values from a system perspective. The heating rates used to calculate  
 188 the permitted fluid temperature change were obtained using the following equation (Taler et al., 2015):

$$\frac{dT_f}{dt} = \frac{p_{\max} v_{T_{\min}} - p_{\min} v_{T_{\max}}}{p_{\max} - p_{\min}} + \frac{v_{T_{\max}} - v_{T_{\min}}}{p_{\max} - p_{\min}} p(T_f) \quad (1)$$

189 These equations express the rate at which the fluid temperature ( $T_f$ ) can change depending on the pressure  
 190 of the fluid (minimum ( $p_{\min}$ ) and maximum ( $p_{\max}$ )) and the minimum and maximum heating rates  
 191 which are dependent on the geometry, material properties and operating temperature and pressure. In an  
 192 evaporator, the water is at saturation point so the pressure and temperature are related. As a consequence,  
 193 the temperature of the fluid will be dependent on the pressure, and Equation (1) can be solved using a

194 Runge-Kutta method, assuming  $T_f(t = 0) = T_0$ . In the case of the super-heater, the fluid is not at  
195 saturation conditions, the pressure is a function of time and determined by the evaporator conditions.

196 Simulations were carried out for different constraints on the evaporator and the super-heater. As discussed  
197 by the authors in Ferruzza et al. (2015), an optimal heating rate constraint can be found for the super-  
198 heater by assuming that it is 1.8 times higher than the evaporator limit. However, simulations were also  
199 carried out using a 1.1 multiplier, to demonstrate the impact of this value and show how sensitive the  
200 results are to this design parameter. Two main start-up schedules can be identified for the evaporator. In  
201 the case of an evaporator with a drum configuration (natural or forced circulation), the minimum  
202 allowable pressure of the steam turbine can be maintained overnight. Such a start-up routine will be  
203 termed a hot start-up. However, when this is not possible (absence of steam drum or pressure vessel), the  
204 pressure would not be maintained overnight and the evaporator would have to start up from ambient  
205 pressure conditions. This will be termed a cold start-up. In order to study how different heating rate  
206 routines will affect the start-up of the power plant, both hot and cold start-ups were included, making the  
207 assumption that the overnight heat losses from the steam drum will be negligible. Observations from  
208 existing power plants indicate that the overnight heat losses from the steam drum may be neglected due to  
209 the large mass of water containing a high thermal inertia and experiencing a limited temperature drop.

### 210 **2.3 Steam turbine start-up schedule**

211 As for the SGS, the steam turbine start-up procedure is limited by the permissible temperature difference  
212 between the metal surface and the steam. Different start-up schedules are defined by the manufacturer  
213 based on the initial temperature of the turbine metal (or stand still time). The start-ups procedures are  
214 classified as cold, warm or hot. A hot start-up would take only 8-10 % of the time it takes for a cold start-  
215 up, while a warm start-up would take 45-50 % of that of a cold start-up (Topel et al., 2015). Figure 2  
216 illustrates the three different start-up curves. The start-up procedure involves two phase which are  
217 denoted for the cold case as the A-B and B-C lines which represent the rolling up and loading up of the  
218 turbine, respectively (Topel et al., 2015).

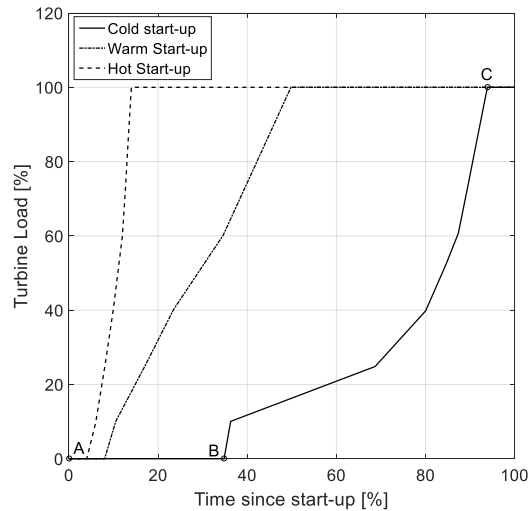


Figure 2: Cold, warm and hot steam turbine start-ups (Adapted from Topel et al., (2015)).

219 The start-up schedules were kept constant in order to focus mostly on the impact of the steam generator  
 220 on the overall performance of the power plant. The minimum allowable pressure was kept at 35 bar (as by  
 221 requirement of the steam turbine) and the rate at which pressure, mass flow rate and temperature could  
 222 rise were determined following the paper by Schenk et al., (2015). During the running-up the mass flow  
 223 rate is kept at 5 % of the nominal value, while during the loading up the mass flow rate increases with a  
 224 rate determined directly by the steam turbine start-up routine depending on the metal temperature at  
 225 which the procedure begins. The different hot, warm and cold start-up curves presented in Figure 2 were  
 226 introduced in the model, depending on the metal temperature (Topel et al., 2015).

## 227 2.4 Power plant modelling

228 The plant layout considered in the paper is shown in Figure 3. The thick lines represent the HTF loop,  
 229 which is heated up by the parabolic trough (PT) mirrors, and either fed directly to the steam generator  
 230 (comprising an economizer (ECO), evaporator (EVA), super-heater (SH) and re-heater (RH)) or to heat-  
 231 up, through the indirect heat exchanger (IHX), the salts from the cold tank (CT) which are then pumped  
 232 to the hot tank (HT). The other cycle represents a conventional Rankine-reheat cycle with high pressure  
 233 (HP) and low pressure (LP) steam turbines (ST) an air-cooled condenser (ACC) and a deaerator (D). The  
 234 power plant was designed for the location of Seville, Spain, with a power output of 55 MWe gross,  
 235 according to Guedez et al. (2017) for the power block, Gilman et al. (2008) for the HTF cycle Lippke  
 236 (1995) and Dudley (1994) for the solar field. Firstly, the Rankine cycle was designed for the chosen gross

237 power, determining its efficiency and thermal input requirement. The size of the solar field was  
238 determined accordingly and scaled considering the solar multiple (SM). Lastly, the thermal energy  
239 storage (TES) mass was calculated to ensure the amount of hours desired to satisfy the thermal demand of  
240 the power block. The design methodology was implemented in Matlab, while the yearly performance  
241 dynamic model was developed in TRNSYS (University of Wisconsin Madison, 1975) in order to be  
242 implemented in DYESOPT.

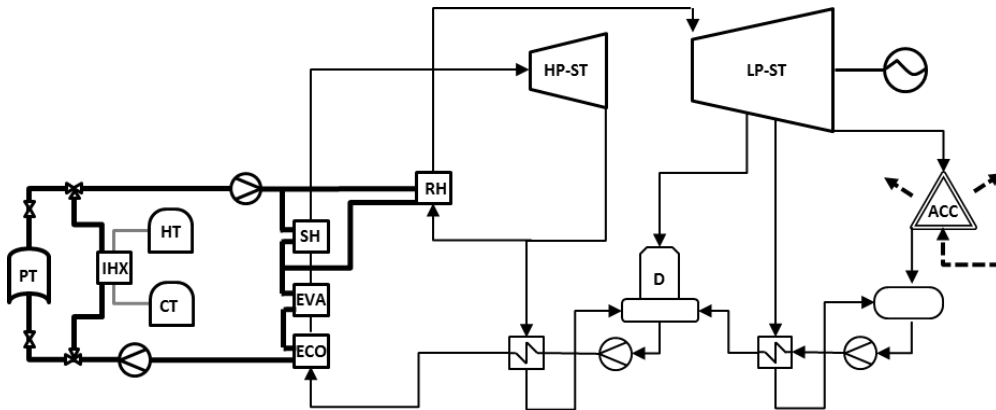


Figure 3: Layout of the considered parabolic trough power plant integrated with indirect thermal energy storage and air cooled condenser.

243 The dynamic model of the power plant was integrated with a controller, which ran the start-up procedure  
244 and applied the constraints to the steam generator and turbine. The logic of the controller is shown in  
245 Figure 4. A similar strategy was applied when the power plant was operating either in solar-driven or  
246 peak-load. In solar-driven, the start-up will occur in the morning as soon as the solar heat is available. In  
247 this case, both the thermal shock and the thermal stresses (in the form of heating rates) are calculated and  
248 a required HTF temperature is sent to the solar field. Afterwards, the steam temperature and pressure rise  
249 accordingly, until the minimum allowable condition for superheated steam is reached. At this point the  
250 steam turbine can start according to the start-up procedure. Similarly, for peak-load operation, the heating  
251 rate constraints are calculated, from which a HTF temperature is obtained. However, as the plant operates  
252 at specific times of the day, an optimal design is supposed to ensure that there is heat available to be  
253 extracted from either the solar field or the thermal storage hot tank. If the thermal storage is used, the oil  
254 temperature can be regulated by adjusting the salt mass flow rate. If HTF temperatures higher than the  
255 allowable SGS HTF temperature occur, an attenuator may be used to reduce the temperature of the  
256 thermal oil or the HTF may be mixed (if possible) with oil at a lower temperature, either from the solar  
257 field loop or the SGS return line. One of the key differences between the two operation modes is the fact

258 that at peak-load the heat is readily available for the SGS and its constraints are the limiting factors, while  
 259 in solar-driven operation mode, the heat availability is dependent on the position of the sun and the size of  
 260 the solar field.

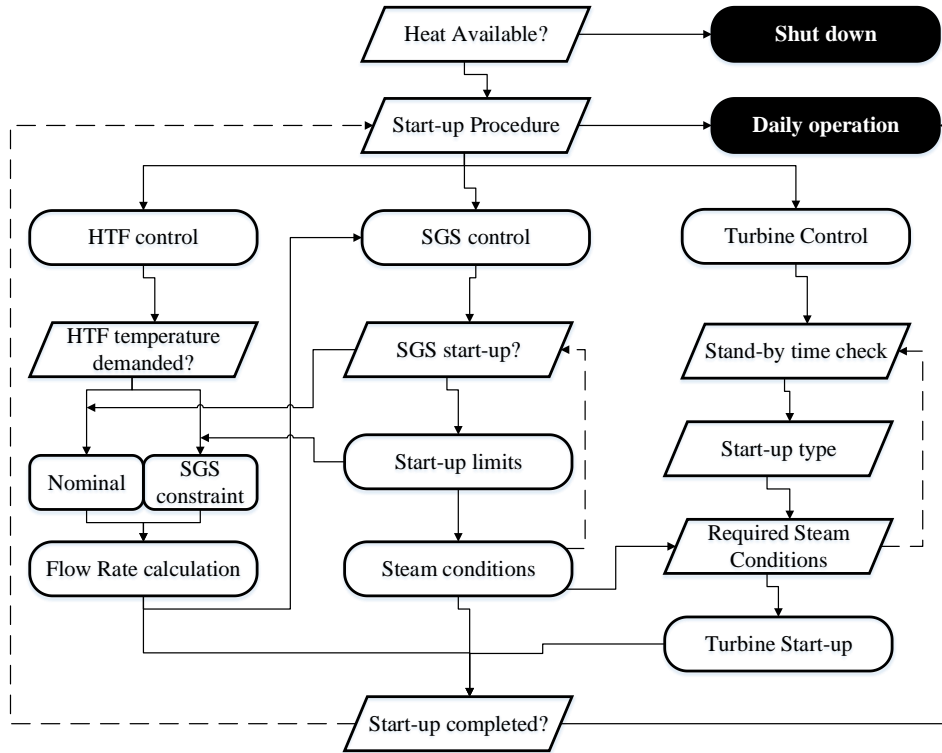


Figure 4: Control logic for the power plant during start-ups.

261 Once both the turbine and the steam generator have reached nominal operating conditions, the start-up  
 262 procedure is finished and the power plant enters daily operation. Part-load operation is taken into account  
 263 according to DLR (2006), if nominal heat input is not reached at the steam generator. The strategy  
 264 depicted in Figure 4 is applicable in both peak-load and solar-driven operation mode. Table 1 summarizes  
 265 the conditions for the two operational modes following Guedez et al. (2017).

Table 1: Summary of operation modes

Operation mode name	Condition
Solar-driven	Whenever radiation or TES are available
Peak-load	Only between 15-21 if heat input is available

266 The main design parameters and thermal performance indicators are listed in Table 2. It summarizes both  
 267 the parameters which were considered fixed and the ones that were allowed to vary for the purpose of the  
 268 analysis. The PTPP designed according to Table 2 served as a basis for an analysis of the impact of the  
 269 constraints. The SM and TES size for the peak-load case were chosen following Guedez et al. (2017). In

270 the solar-driven case the SM was varied to account for the impact of the solar field size while the TES  
 271 was kept at 10 h as this was a size that would still require warm turbine start-ups while allowing the plant  
 272 to operate in the evening even in winter periods. The 15-21 time operation was chosen according to  
 273 Guedez et al. (2017). However, in Guedez et al. (2017) the price of electricity in the suggested location  
 274 was higher than zero even between 5 and 17. The study considered only peak price hours, in order to  
 275 remove the influence of the solar field on the SGS. This means that the heat provided to the steam  
 276 generator comes directly either only from the TES or from the combination of the TES and SF, in case it  
 277 cannot come directly from the solar input. If the DNI is high enough the PT has already gone through its  
 278 start-up phase and could potentially provide nominal heat input to the steam generator. This makes it  
 279 possible to focus on how the constraints of the evaporator and super-heater affect the performance of the  
 280 power plant if electricity production was postponed to a particular time of the day.

Table 2: Summary of design parameters

Operation mode name	Units	Peakload case	Solar-driven case
SM	[-]	1.1	1.5-3
Gross Power	[MW]	55	55
TES capacity	[h]	5	10
Inlet HP/LP pressure	[bar]	100/16.7	100/16.7
Nominal condensing pressure	[bar]	0.06	0.06
SF HTF maximum temperature	[°C]	393	393
Nominal turbine inlet temperature	[°C]	378	378

### 281 3 Results and discussion

282 The impact of the start-up constraints was investigated and the performance of the power plant under  
 283 different limitations is presented in this section. Both peak-load and solar-driven operation were analysed.  
 284 For both of these modes, the start-up constraint of the steam generator was analysed for the cases shown  
 285 in Table 3.

Table 3: Summary of the respective parameters for the four different cases analyzed.

Case Name	Case 1 a/b	Case 2 a/b	Case 3 a/b	Case 4 a/b
Average evaporator heating rate [K/min]	3-12	3-12	3-12	3-12
Super-heater heating rate multiplier [K/min]	1.1/1.8	1.1/1.8	1.1/1.8	1.1/1.8
Start pressure [bar]	35	1	35	1
Thermal shock $\Delta T$ [K]	63	63	63	63
Operation strategy	peakload	peakload	solar-driven	solar-driven

286 The lower threshold for evaporator constraints was chosen as a reference, representing a slow start-up of  
 287 the SGS system (Pelagotti et al., 2014). This constraint can be considered as representative of a steam

288 generator system based on a kettle-reboiler type evaporator (González-Gómez et al., 2017). The higher  
289 threshold was chosen as a potential improvement compared with the designs of header and coil  
290 geometrical configurations already available in industry (Aalborg CSP, 2015). The cases are also  
291 considering different start-up strategies for the steam generator. If a hot start-up is available (Case 1 and  
292 Case 3 respectively), it means that the minimum allowable pressure of the turbine is kept at the steam  
293 drum. In the case of a cold start-up (Case 2 and Case 4 respectively), the pressure starts from ambient  
294 conditions.

### 295 **3.1 Peak-load case**

296 Figure 5 shows the results of the impact of the SGS heating rate constraints on the yearly electricity  
297 production for the cases presented in Table 3. The graph indicates that for a hot start-up, the potential  
298 improvement in Case 1 is 1.54 % (0.9 GWhe) for Case 1a. For cold start-ups of the evaporator, the  
299 potential increases to 12.5 % (6.3 GWhe). Higher impacts were found for Cases 1b and 2b, when lower  
300 SH heating rate multipliers were chosen, the potential for improvement being as high as 3.6 % and 25 %.  
301 In the first cases, the evaporator was the main limiting factor during the start-up, while in the latter the  
302 limitations imposed on the super-heater delayed the initial phase of the turbine start-up, making the  
303 impact of the procedure more significant in terms of electricity production. These findings demonstrate  
304 the importance of a properly designed and operated super-heater while starting up the SGS. The results of  
305 Case 1a suggest that for hot evaporator start-ups it is possible to identify an optimal range of heating rate  
306 constraints around 7-8 K/min. Beyond this threshold, no significant increase in power production was  
307 observed, making it unnecessary to go above this design point. This is mainly due to the fact that even  
308 though the SH could reach its nominal operating condition at faster rates, the turbine would still have to  
309 be operated so as to respect its thermal limitations. This underlines how significant it is to consider both  
310 components when optimising the total system design to respect thermo-mechanical constraints. If a faster  
311 start-up rate was achievable for the steam turbine, then higher start-up constraints would be required for  
312 the steam generator. For a cold start-up of an evaporator, higher start-up rates would always imply greater  
313 electricity production for both a slow and a fast super-heater. In fact, the pressure that could be  
314 maintained overnight was well below the minimum allowable pressure for the steam turbine, requiring  
315 that SGS covers a larger temperature gradient, in turn postponing the beginning of the steam turbine start-  
316 up.

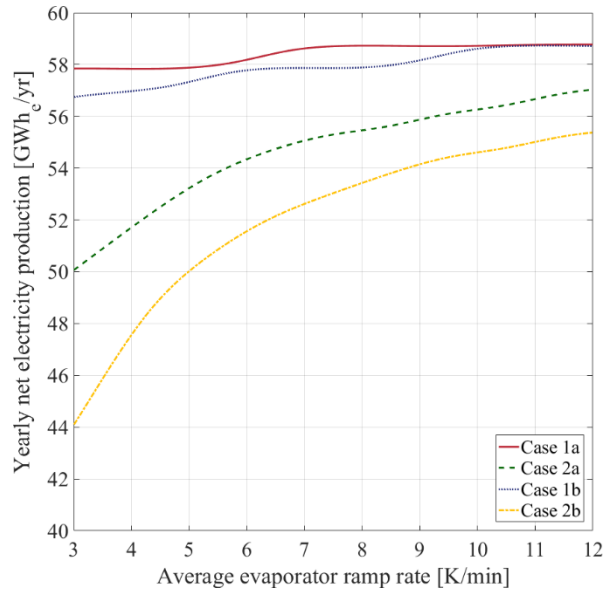


Figure 5: Impact of the evaporator heating rate constraints on the net electricity production for a peak-load operating strategy.

317 Figures 6a and 6b show respectively the steam temperature during a two day period and the net  
 318 electricity output for case 1a. The two different lines refer to a slow (3 K/min) and a fast (12 K/min) SGS  
 319 configuration. Figures 7a and 7b show the same variables but for case 2a. The results illustrated in Figure  
 320 5 may better understood by looking at Figures 6 and 7. In the first two, it may be seen that even if the  
 321 evaporator start-up rate is 4 times higher than in the slow case, the impact on the net power output is  
 322 barely noticeable (a close up is shown in the left part of the graph). This means that every day the  
 323 beginning of the steam turbine start-up procedure is delayed by 6 minutes. In case 2, on the other hand, if  
 324 the steam pressure is not maintained overnight, the delay is more significant and observable. In this case  
 325 the steam turbine would experience a delay of as much as 30 minutes, making the SGS a bottleneck for  
 326 the start-up procedure. These considerations indicate that the presence of a pressure vessel (in the form of  
 327 a steam drum in this case) is important, to make the start-up procedure as effective as possible.



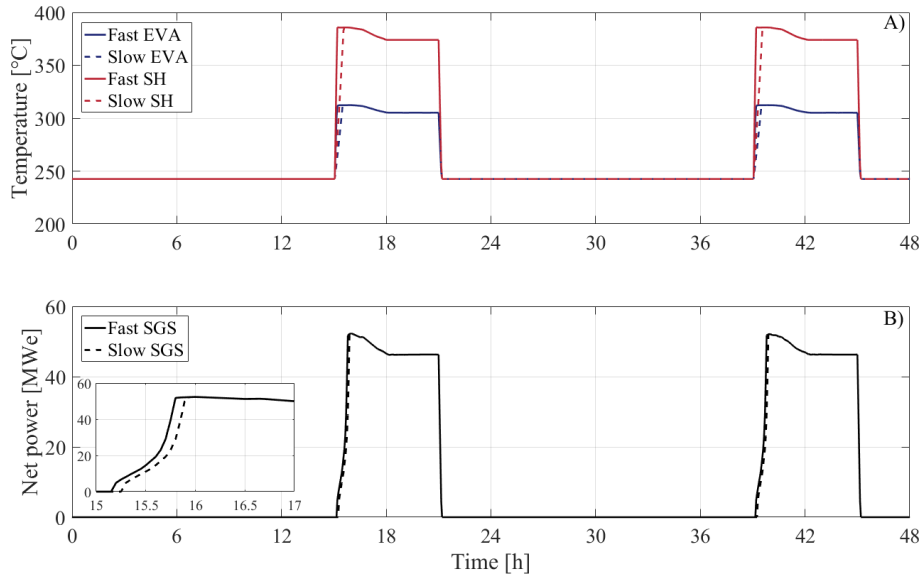


Figure 6: Comparison of a two-day performance between a slow and a fast evaporator during a hot start-up for a peak-load operating strategy case. A) Evaporator and superheater temperatures, B) Net power output.

328

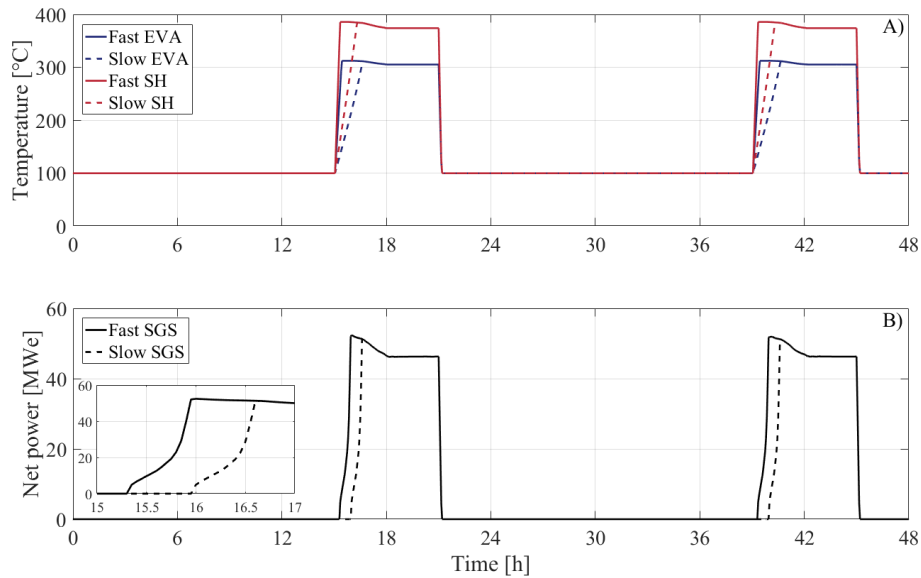


Figure 7: Comparison of a two-day performance between a slow and a fast evaporator during a cold start-up for a peak-load operating strategy case. A) Evaporator and superheater temperatures, B) Net power output.

329

330 **3.2 Solar-driven case**

331 Figure 8 illustrates an analysis similar to the one described in section 3.1 but for a solar-driven  
 332 operational strategy. The reference case adopted was for a SM equal to 2, being a representative value for  
 333 existing power plant configurations like Andasol (Ferruzza et al., 2017). Following a similar  
 334 consideration as before, if only hot evaporator start-ups are considered, the results indicate that the  
 335 potential for improvement of the net electricity production is as low as 0.27 % (0.56GWh<sub>e</sub>), while for  
 336 cold start-ups, this impact increases to a maximum of 2.3 %. As in the previous case, if the super heater is  
 337 not operated or designed optimally, the maximum potential improvement is 4.65 % for cold start-ups.

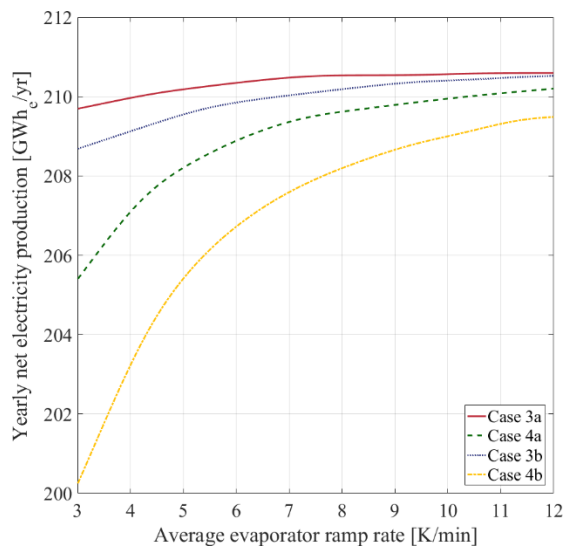


Figure 8: Impact of the evaporator ramp rate on the net electricity production for a solar-driven operating strategy case, considering a solar multiple equal to 2.

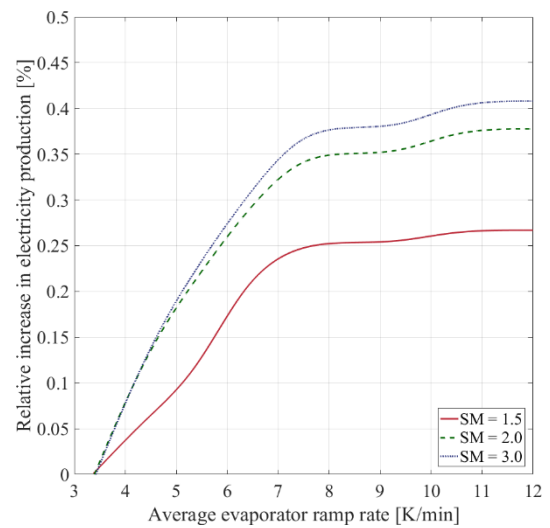


Figure 9: Sensitivity to the solar field size on the impact of the evaporator ramp rate constraints for a solar-driven operating strategy case.

338 Figure 9 illustrates the relative increase in electricity production for different Solar Multiple (SM) cases.  
 339 The figure suggests that the impact of the start-up constraints on the steam generator is considerably  
 340 affected by the size of the solar field. It may be seen that by doubling the size of the solar field from a SM  
 341 of 1.5 to 3.0, the relative increase can be improved from a maximum of 0.28 % to 0.41 %. However, the  
 342 impact is not very important in the economy of the power plant. Figure 10 illustrates the development of  
 343 the solar field thermal output and thermal input to the SGS and may suggest some reasons for this low  
 344 improvement. The close-up in the figure shows that in the morning, the heat input to the SGS follows the

345 same trend as the solar field output, as no storage is available. This means that to reach the nominal  
346 operating condition of thermal output takes roughly 1 hour.

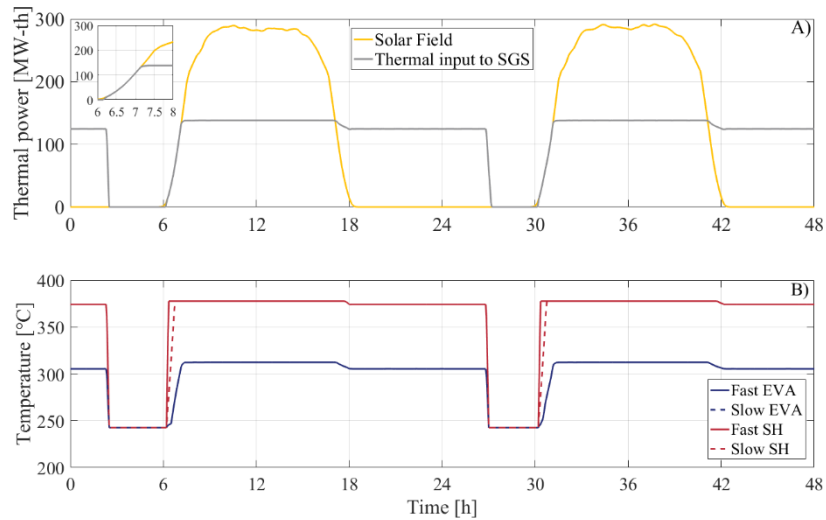


Figure 10: Comparison of a two-day performance between a slow and a fast evaporator during a hot start-up for a solar-driven operating strategy case. A) Thermal power at solar field and input to the steam generator system, B) Evaporator and Super-heater temperatures

347 The pressure at the SGS follows a similar trend, as it is proportional to the heat input to the evaporator.  
348 Hence the start-up at the evaporator is no longer limited by its thermo-mechanical constraints but more by  
349 the heat available from the solar field. This is directly shown in in the lower part of Figure 10. It may be  
350 seen that in both the slow and fast cases, the temperature at the evaporator (and therefore the pressure, as  
351 it is at saturation point), are not two separate lines but they overlap. The only limiting component from a  
352 thermo-mechanical standpoint is therefore the super-heater, resulting in only negligible differences in  
353 power production. In these cases the steam reaches the minimum allowable conditions at a later stage,  
354 delaying the start-up of the turbine.

#### 355 4. Conclusions

356 A detailed analysis was used to illustrate the impact of the SGS constraints during the start-up procedure  
357 of a PTPP. To achieve this, an existing detailed model of a PTPP that had previously been developed by  
358 the authors was extended to allow the simulation of two different operating strategies, namely peak-load  
359 and solar-driven operation. The model was also extended by the addition of an air-cooled condenser. A  
360 simulation tool was used to apply the start-up constraints of both the steam generator and the turbine. The

361 model was integrated with an existing tool for the dynamic performance evaluation of power plants  
362 (DYESOFT).

363 The results suggest that for peak-load operation, by changing the constraints of the steam generator from  
364 3 K/min to 12 K/min, the potential improvement in total net electricity output is 1.5 %. It was shown that  
365 being able to maintain the minimum allowable turbine pressure overnight would be highly beneficial as it  
366 makes it possible to start the steam turbine in the most efficient way. The optimal range of maximum  
367 allowable heating rate for the evaporator was found to be about 7-8 K/min, designing a component with  
368 higher constraints would provide no benefit for the economy of the power plant. For solar-driven  
369 operation, the results indicate that for a solar field design with a SM equal to 2, the potential improvement  
370 of electricity production is as low as 0.27 %. This figure might increase if the SF is further oversized, but  
371 only to 0.41 %. The main limiting factor during start-ups is the amount of heat available in the solar field.  
372 As the solar field can only provide nominal operating power to the SGS after 1 hour, the pressure at the  
373 evaporator cannot achieve its nominal value before that time, so the heating rate will be slower than the  
374 maximum limits in most start-up procedures. As a general conclusion, the results indicate that raising the  
375 maximum allowable evaporator constraints would not proportionally increase the yield of the power  
376 plant, as their effect is limited, either by other constraints at the steam turbine or at the solar field. It is  
377 therefore clear that the interaction among the three components is crucial when optimising the thermo-  
378 mechanical design of an SGS.

379

380 **References**

- 381 Abed, W., Al-maliki, K., Alobaid, F., Kez, V., Epple, B., 2016. Modelling and dynamic simulation of a  
382 parabolic trough power plant. *J. Process Control* 39, 123–138.  
383 <https://doi.org/10.1016/j.jprocont.2016.01.002>
- 384 Almasabi, A., Alobaidli, A., Zhang, T.J., 2015. Transient characterization of multiple parabolic trough  
385 collector loops in a 100 MW CSP plant for solar energy harvesting. *Energy Procedia* 69, 24–33.  
386 <https://doi.org/10.1016/j.egypro.2015.03.004>
- 387 Basaran, I., 2015. A Comprehensive Study of the Imposed Limitations on Concentrating Solar Power  
388 Plant Start-up Speeds. MSc, Thesis. Royal Institute of Technology (KTH), Stockholm.
- 389 Blanco, D., Luis, A., Garcı, I.L., 2011. Performance model for parabolic trough solar thermal power  
390 plants with thermal storage : Comparison to operating plant data. *Sol. Energy* 85, 2443–2460.  
391 <https://doi.org/10.1016/j.solener.2011.07.002>
- 392 CEN, 2012. Water-tube boilers and auxiliary installations - Part 3: Design and calculation for pressure  
393 parts of the boiler. Brussels.
- 394 Conrado, L.S., Rodriguez-pulido, A., Calderón, G., 2017. Thermal performance of parabolic trough solar  
395 collectors. *Renew. Sustain. Energy Rev.* 67, 1345–1359. <https://doi.org/10.1016/j.rser.2016.09.071>
- 396 DLR, 2006. A TRNSYS Model Library for Solar Thermal Electric Components ( STEC ), Reference  
397 manual.
- 398 Dudley, V., 1994. SEGS LS-2 Solar Collector. Test Results. Sandia National Laboratories. Albuquerque,  
399 New Mexico.
- 400 Dzierwa, P., Taler, D., Trojan, M., Taler, J., 2016. Evaporator Heating with Optimum Fluid Temperature  
401 Changes. *Procedia Eng.* 157, 29–37. <https://doi.org/10.1016/j.proeng.2016.08.334>
- 402 Dzierwa, P., Taler, J., 2014. Optimum Heating of Pressure Vessels With Holes. *J. Press. Vessel Technol.*

403 137, 11202. <https://doi.org/10.1115/1.4027584>

404 Ferruzza, D., Topel, M., Basaran, I., Laumert, B., Haglind, F., 2017. Start-Up Performance of Parabolic  
405 Trough Concentrating Solar Power Plants, in: AIP Conference Proceedings 1850. pp. 1–9.  
406 <https://doi.org/10.1063/1.4984542>

407 Gilman, P., Laboratory, N.R.E., Laboratories, S.N., 2008. Solar advisor model user guide for version 2.0.  
408 Technical Report.

409 González-Gómez, P.Á., Gómez-Hernández, J., Briongos, J.V., Santana, D., 2017a. Thermo-economic  
410 optimization of molten salt steam generators. *Energy Convers. Manag.* · 146, 228–243.  
411 <https://doi.org/10.1016/j.enconman.2017.05.027>

412 González-Gómez, P.Á., Petrakopoulou, F., Briongos, J.V., Santana, D., 2017b. Steam generator design  
413 for solar towers using solar salt as heat transfer fluid, in: AIP Conference Proceedings. pp. 1–8.  
414 <https://doi.org/10.1063/1.4984363>

415 Guedez, R., Topel, M., Ferragut, F., Callaba, I., Perez-segarra, C.D., 2017. A Methodology for  
416 Determining Optimum Solar Tower Plant Configurations and Operating Strategies to Maximize  
417 Profits Based on Hourly Electricity Market Prices and Tariffs. *Sol. Energy Eng.* 138, 1–12.  
418 <https://doi.org/10.1115/1.4032244>

419 International Energy Agency, 2014. Technology Roadmap, Solar Thermal Electricity. Paris.

420 Lippke, F., 1995. Simulation of the Part-Load Behavior of a 30 Mwe SEGS Plant. Report. Sandia  
421 National Laboratories. Albuquerque, New Mexico.

422 Luo, N., Yu, G., Hou, H.J., Yang, Y.P., 2015. Dynamic modeling and simulation of parabolic trough solar  
423 system, in: SolarPACES 2014. pp. 1344–1348. <https://doi.org/10.1016/j.egypro.2015.03.137>

424 Moore, J., Grimes, R., O'Donovan, A., Walsh, E., 2013. Design and testing of a novel air-cooled  
425 condenser for concentrated solar power plants. *Energy Procedia* 49, 1439–1449.  
426 <https://doi.org/10.1016/j.egypro.2014.03.153>

- 427 Pelagotti, L., Sørensen, K., Condra, T.J., Joseph, T., Franco, A., 2014. Modelling of a Coil Steam  
428 Generator for CSP applications \$, in: Proceedings of the 55th International Conference on  
429 Simulation and Modelling.
- 430 Price, J.W.H., 2017. Thermal Shock Cracking : Design and Assessment Guidelines Thermal Shock  
431 Cracking : Design and Assessment Guidelines. J. Press. Vessel Technol. 129, 125–132.  
432 <https://doi.org/10.1115/1.2389029>
- 433 Samanes, J., Garcia-barberena, J., 2014. A model for the transient performance simulation of solar cavity  
434 receivers. Sol. Energy 110, 789–806. <https://doi.org/10.1016/j.solener.2014.10.015>
- 435 Schenk, H., Dersch, J., Hirsch, T., Polklas, T., 2015. Transient Simulation of the Power Block in a  
436 Parabolic Trough Power Plant. Proc. 11 Int. Model. Conf. 605–614.  
437 <https://doi.org/10.3384/ecp15118605>
- 438 Spelling, J., Jöcker, M., Martin, A., 2012. Annual performance improvement for solar steam turbines  
439 through the use of temperature-maintaining modifications. Sol. Energy 86, 496–504.  
440 <https://doi.org/10.1016/j.solener.2011.10.023>
- 441 Taler, J., Weglowski, B., Taler, D., Sobota, T., Dzierwa, P., Trojan, M., Madejski, P., Pilarczyk, M.,  
442 2015. Determination of start-up curves for a boiler with natural circulation based on the analysis of  
443 stress distribution in critical pressure components. Energy 92, 153–159.  
444 <https://doi.org/10.1016/j.energy.2015.03.086>
- 445 Thermoflow, 2014. Thermoflex Modular Program for Thermal Power Sys- tems [WWW Document].  
446 URL [www.thermoflow.com](http://www.thermoflow.com) (accessed 11.22.17).
- 447 Topel, M., Genrup, M., Jöcker, M., Spelling, J., Laumert, B., 2017. Operational Improvements for Startup  
448 Time Reduction in Solar Steam Turbines. Sol. Energy Eng. 137, 1–8.  
449 <https://doi.org/10.1115/1.4028661>
- 450 Topel, M., Guédez, R., Laumert, B., 2015. Impact of Increasing Steam Turbine Flexibility on the Annual

451 Performance of a Direct Steam Generation Tower Power Plant. Energy Procedia 69, 1171–1180.  
452 <https://doi.org/10.1016/j.egypro.2015.03.196>

453 University of Wisconsin Madison. Solar Energy Laboratory., 1975. TRNSYS, a transient simulation  
454 program. Madison, Wis. : The Laboratory, 1975.

455 Vant-Hull, L.L., 2012. Central tower concentrating solar power (CSP) systems, Concentrating Solar  
456 Power Technology: Principles, Developments and Applications. Woodhead Publishing Limited,  
457 Houston. <https://doi.org/10.1016/B978-1-84569-769-3.50008-X>

458 Aalborg CSP, 2015. Aalborg CSP Steam Generator. URL  
459 <http://www.aalborgcsp.com/quickmenu/brochures/> (accessed 8.3.17).

460